Collapse of Magnetized Singular Isothermal Toroids: II. Rotation and Magnetic Braking

Anthony Allen

Institute of Astronomy and Astrophysics, Academia Sinica, PO BOX 23-141, Taipei 106, Taiwan, R.O.C.

Zhi-Yun Li

Department of Astronomy, University of Virginia, Charlottesville, VA 22903

Frank H. Shu

National Tsing Hua University, 101, Section 2 Kuang Fu Road, Hsinchu, Taiwan 300, R.O.C.

ABSTRACT

We study numerically the collapse of rotating, magnetized molecular cloud cores, focusing on rotation and magnetic braking during the main accretion phase of isolated star formation. Motivated by previous numerical work and analytic considerations, we idealize the pre-collapse core as a magnetized singular isothermal toroid, with a constant rotational speed everywhere. The collapse starts from the center, and propagates outwards in an inside-out fashion, satisfying exact self-similarity in space and time. For rotation rates and field strengths typical of dense low-mass cores, the main feature remains the flattening of the mass distribution along field lines – the formation of a pseudodisk, as in the nonrotating cases. The density distribution of the pseudodisk is little affected by rotation. On the other hand, the rotation rate is strongly modified by pseudodisk formation. Most of the centrally accreted material reaches the vicinity of the protostar through the pseudodisk. The specific angular momentum can be greatly reduced on the way, by an order of magnitude or more, even when the pre-collapse field strength is substantially below the critical value for dominant cloud support. The efficient magnetic braking is due to the pinched geometry of the magnetic field in the pseudodisk, which strengthens the magnetic field and lengthens the level arm for braking. Both effects enhance the magnetic transport of angular momentum from inside to outside. The excess angular momentum is carried away in a low-speed outflow that has, despite claims made by other workers, little in common with observed bipolar molecular outflows. We discuss the

implications of our calculations for the formation of true disks that are supported against gravity by rotation.

Subject headings: accretion — ISM: clouds — magnetohydrodynamics — stars: formation

1. Introduction

Rotation is observed ubiquitously in star-forming cores. On the scale of $\sim$0.1 pc, the detected rotation rate is small, with a typical value corresponding to a ratio of rotational to gravitational energy of 0.02 (Goodman et al. 1993). The rotation rate is much lower than expected if the core is condensed out of a low density background medium with angular momentum conserved. The slow core rotation is thought to be due to magnetic braking (Mestel 1985; Mouschovias & Ciolek 1999), which is particularly efficient during the long, magnetically subcritical phase of cloud evolution driven by ambipolar diffusion (Basu & Mouschovias 1994). This assumes that the clouds are strongly magnetized to begin with, as envisioned in the standard picture of isolated low-mass star formation (Shu, Adams & Lizano 1987). Once a magnetically supercritical core develops, it begins to collapse dynamically. It is often assumed that magnetic braking then becomes inefficient, with most of the angular momentum of the core material carried by the collapsing flow into the central star-plus-disk or binary system. However, the typical value of specific angular momentum inferred for dense cores is an order of magnitude higher than the typical binary value, at least in the Taurus cloud complex (see Fig. 8 of Simon et al. 1995 and discussion in § 8.5 of Myers 1995). This suggests that a large fraction of the core angular momentum may still be removed *during collapse*. The problem of angular momentum redistribution in a collapsing magnetized core thus warrants a closer examination.

The efficiency of magnetic braking depends sensitively on the magnetic field geometry (Mestel 1985). The exact field geometry of a magnetized core on the verge of collapse is difficult to determine without following the cloud evolution in three dimensions. Simplified numerical calculations of cloud evolution driven by ambipolar diffusion have shown, however, that by the time a central density cusp is formed the mass-to-flux ratio is approximately spatially constant in the supercritical core, and the (volume) density decreases with radius roughly as a power-law of r^{-2} (Lizano & Shu 1989; Basu & Mouschovias 1994). This self-similar behavior motivated Li & Shu (1996) to idealize the end state of the ambipolar diffusion-driven core formation as a scale-free configuration supported in part by a large scale magnetic field and in part by the thermal pressure gradient, with a fixed mass-to-flux ratio and an exact r^{-2} density profile. Such a configuration turns out to be a singular

isothermal toroid, for which the magnetic field geometry can be computed exactly (see also Baureis, Ebert, & Schmitz 1989). The field geometry is distorted by fluid motions during the subsequent inside-out collapse.

In a companion paper to this journal (Allen, Shu & Li 2003; hereafter Paper I), we have studied the collapse of magnetized, singular isothermal toroids without rotation. The main features of the collapse solution are governed by the anisotropy in the magnetic forces, which induces in the toroid an evacuated region near the axis, where the plasma β parameter (the ratio of thermal to magnetic energy density) drops below unity (see Fig. 4a of Paper I). As the core collapses from inside out, matter in the magnetically dominated region slides along the field lines towards the equatorial region, creating a dense, flattened structure – a pseudodisk (Galli & Shu 1993a,b). The material in the pseudodisk collapses radially towards the central point mass in a magnetically diluted free-fall, dragging the footpoints of field lines along with it (see Fig. 4b of Paper I). A highly pinched field configuration ("split monopole") is produced, with important implications for the magnetic transport of angular momentum from inside to outside. In the presence of rotation, the collapse would lead to a spinup of the pseudodisk, which is linked magnetically to a more slowly rotating envelope of infalling and nearly static material. We will show in this paper that the twisting of magnetic field lines actually drives a slow outflow during the core collapse, which can remove much of the angular momentum remaining in the infalling pseudodisk. This removal poses a substantial brake against the eventual formation of a centrifugally supported disk unless the trapped magnetic field is lost in the realistic situation by nonideal MHD effects.

As the first step toward the dynamical calculations, we will generalize the magnetized, singular isothermal toroid solutions of Li & Shu (1996) to include rotation in § 2. These magnetized rotating toroids are then induced to collapse from inside out in § 3, and the collapse is followed numerically in a manner similar to that described in Paper I. The numerical solutions are discussed in § 4, with an emphasis on the efficiency of magnetic braking during core collapse and the implications for the difficulty of forming rotationally supported disks unless significant flux loss appears in the realistic problem at small scales, as is expected theoretically for high-density situations (e.g., Nishi, Nakano & Umebayashi 1991; Desch & Mouschovias 2001). We end with a brief summary and conclusion in § 4.4.

2. Magnetized, Rotating Singular Isothermal Toroids

2.1. Governing Equations

We consider a rotating, scale-free (self-similar), self-gravitating cloud that is magnetized by a purely poloidal field and in mechanical force balance. The cloud is specified by the mass density ρ, the magnetic flux function Φ which determines the poloidal field through $2\pi\mathbf{B} = \nabla \times [(\Phi/r\sin\theta)\mathbf{e}_\varphi]$, and the rotational speed u_φ, in a spherical polar coordinate system (r, θ, φ). Under the assumption of axisymmetry, the radial and angular dependences of these cloud quantities can be separated, on dimensional grounds, into

$$\rho(r,\theta) = \frac{a^2}{2\pi G r^2} R(\theta), \tag{1}$$

$$\Phi(r,\theta) = \frac{4\pi a^2 r}{G^{1/2}} \phi(\theta), \tag{2}$$

$$u_\varphi(r,\theta) = a\ v(\theta), \tag{3}$$

where a is the isothermal sound speed, which we take to be a constant, and the functions $R(\theta)$, $\phi(\theta)$ and $v(\theta)$ describe the angular distributions of the density, magnetic flux, and rotational speed.

In order to be in a mechanical force balance, the cloud must satisfy the momentum equation,

$$\rho\left[\nabla\left(\frac{u_\varphi^2}{2}\right) + (\nabla\times\mathbf{u})\times\mathbf{u}\right] = -\rho\nabla V - \nabla P + \frac{1}{4\pi}(\nabla\times\mathbf{B})\times\mathbf{B}, \tag{4}$$

where $P = \rho a^2$ is the thermal pressure, and the velocity $\mathbf{u} = u_\varphi\mathbf{e}_\varphi$ has only a toroidal component. The gravitational potential V is related to the density through Poisson's equation

$$\nabla^2 V = 4\pi G\rho. \tag{5}$$

It can be decomposed into a form (Toomre 1982)

$$V(r,\theta) = 2a^2(1+H_0)[\ln r + h(\theta)], \tag{6}$$

where H_0 is the fractional over-density of the (rotating) magnetized configuration over the singular isothermal sphere that was introduced by Li & Shu (1996). This overdensity arises from a combination of magnetization and rotation. The angular function $h(\theta)$ is equivalent to the function $P(\theta)$ of Toomre (1982; see his equation [7]).

Substituting equations (1), (2), (3) and (6) into equations (4) and (5) and eliminating the function $h(\theta)$ yield two coupled second-order ordinary differential equations (ODEs) for the angular distributions of density, $R(\theta)$, and magnetic flux, $\phi(\theta)$,

$$\frac{d}{d\theta}\left[\sin\theta\left(-\frac{1}{R}\frac{dR}{d\theta}-\frac{v^2-2H_0}{\phi}\frac{d\phi}{d\theta}+\frac{v^2\cos\theta}{\sin\theta}\right)\right]=2(R-1-H_0)\sin\theta, \tag{7}$$

$$\frac{d}{d\theta}\left(\frac{1}{\sin\theta}\frac{d\phi}{d\theta}\right)=\frac{R\sin\theta}{2\phi}(v^2-2H_0), \tag{8}$$

where the angular distribution of rotational speed $v(\theta)$ remains to be determined. In the nonrotating limit that $v(\theta)=0$, these two coupled ODEs reduce to equations (12) and (13) of Li & Shu (1996).

The eliminated function $h(\theta)$ that appears in the expression for gravitational potential, equation (6), is related to other functions by

$$\frac{dh}{d\theta}=\frac{1}{2(1+H_0)}\left[-\frac{1}{R}\frac{dR}{d\theta}-\frac{v^2-2H_0}{\phi}\frac{d\phi}{d\theta}+\frac{v^2\cos\theta}{\sin\theta}\right]. \tag{9}$$

2.2. Non-Magnetic Limit

In the nonmagnetic limit $\phi(\theta)\to 0$, equation (8) demands that $v(\theta)=\sqrt{2H_0}$, i.e., constant rotational speed everywhere. It is easy to verify the remaining two governing equations, (7) and (9), reduce to equations (15) and (16) of Toomre (1982; see also Hayashi, Narita & Miyama 1982), with slightly different notations. In this purely rotating case, Toomre (1982) gave an exact solution for the angular distribution of density, which in our notation becomes

$$R(\theta)=(1+H_0)^2\cosh^2\xi\ \mathrm{sech}^2[(1+H_0)\xi], \tag{10}$$

where the new variable ξ is related to the polar angle θ through $\tanh\xi=\cos\theta$. Equation (10) describes the so-called "Toomre-Hayashi toroid".

2.3. Generalized Toroid Solutions

In the general case, both the flux function $\phi(\theta)$ and the rotation speed $v(\theta)$ are nonzero. This creates a potential problem, because fluid parcels along a given field line will generally wrap up the field, introducing a toroidal component that redistributes the fluid angular momentum, unless the angular speed $\Omega(r,\theta)$ is constant along the field line (i.e., matter and magnetic field corotate). The result follows from field freezing, i.e., the induction equation

of ideal MHD, which we have yet to consider, coupled with the condition $\nabla \cdot \mathbf{B} = 0$. Applied to an axisymmetric configuration of poloidal field lines, the presence of axial rotation, $u_\varphi \equiv r\Omega \sin\theta$, will lead to a generation of a toroidal component at a rate:

$$\frac{\partial B_\varphi}{\partial t} = r \sin\theta \left[B_r \frac{\partial \Omega}{\partial r} + \frac{B_\theta}{r} \frac{\partial \Omega}{\partial \theta} \right]. \tag{11}$$

For there to be no toroidal field generation or change, the right-hand side has to be zero, i.e., $\mathbf{B} \cdot \nabla \Omega = 0$, which is the requirement of isorotation on field lines (Ferraro 1937). In a self-similar toroid, isorotation requires

$$v(\theta) = \frac{C \sin\theta}{\phi(\theta)}, \tag{12}$$

where C is a constant.

Unfortunately, self-similar magnetic field lines providing nontrivial cloud support extend infinitely far in cylindrical radius $r \sin\theta$. If Ω were to remain a nonzero constant as $r \sin\theta \to \infty$ on a field line, then the linear rotational speed $u_\varphi = r\Omega \sin\theta$ would increase without bound. The resulting divergent centrifugal force cannot be balanced by any combination of the other self-similar forces in the problem. Differential rotation along a field line is therefore unavoidable if the unbounded cloud is to start in mechanical force balance everywhere. Alternatively, we may say that if Ω has a nonzero constant value on a field line, then the quantity a/Ω would yield an intrinsic length scale, and we would have to give up the simplifying assumption of self-similarity. We choose to retain exact self-similarity and forego instead isorotation on field lines.

Differential rotation along a field line, $\mathbf{B} \cdot \nabla \Omega \neq 0$ at the initial (pivotal) instant $t = 0$, extracts a price, and that price is an instantaneous wrapping of the magnetic field for $t > 0$ via equation (11). The spontaneous generation of toroidal field is an inevitable consequence of differential rotation in the problem, so one might wonder why we do not include a systematic toroidal field at the outset in the pivotal state. We do not do so for three reasons. First, it would introduce arbitrary extra parameters into a problem that is already sufficiently complex. Second, axisymmetric models that contain toroidal fields which extend infinitely in the axial direction (e.g., Fiege & Pudritz 2000) generally have undesirable unclosed systems of currents that lead to large-scale separations of electric charge over time. Third, observations of millimeter-wave and far infrared polarization patterns do not indicate substantive toroidal fields in the noncollapsing portions of molecular and dark clouds (see, e.g., Ward-Thompson et al. 2000 for the case of starless core L1544).

In our problem, the spatially limited generation of a finite level of B_φ slowly throws the cloud out of mechanical equilibrium in the poloidal directions. We regard this feature of the

solutions to be less important than the fast poloidal motions that are generated because the pivotal state is unstable to inside-out dynamical collapse. Thus, we shall focus our attention for $t > 0$ on the magnetic torques exerted on exterior material connected to field lines dragged into a rotating, collapsing pseudodisk. We shall find the back reaction of those torques on the infalling material to be a formidable magnetic brake working against the formation of centrifugally supported disks.

A simple way to introduce the necessary degree of differential rotation into the equilibrium toroid is to multiply the expression for $v(\theta)$ in equation (12) by an extra factor of $\sin(\theta)$, so that

$$v(\theta) = \frac{C \sin^2 \theta}{\phi(\theta)}. \tag{13}$$

We have checked by direct computation that models satisfying equation (13) have finite rotation speeds everywhere, with a moderate angular variation. The above choice is arbitrary, however, and a simpler, esthetically more appealing alternative is a constant rotational speed v independent of θ. This choice for the pivotal state is suggested by the pre-pivotal evolutionary calculations of Basu & Mouschovias (1994) including both ambipolar diffusion and rotation. The choice also has the advantage of describing the Toomre-Hayashi toroid in the nonmagnetic limit. Collapse calculations computed with pivotal states satisfying equation (13) yield results that are qualitatively similar to the cases with $v = \text{const}$. In addition, self-gravitating isothermal configurations with flat rotation curves have a long respected tradition in observational astronomy and theoretical astrophysics, with generalizations even possible into the relativistic regime (Cai & Shu 2002, 2003) and for nonaxisymmetric equilibria (Syer & Tremaine 1996, Galli et al. 2001).

With $v = \text{const} \equiv v_0$, we can now cast the two coupled second-order ODEs (7) and (8) into a set of four first-order ODEs

$$\frac{dS}{d\theta} = 2 \sin\theta (R - H_0 - 1), \tag{14}$$

$$\frac{dT}{d\theta} = \frac{R \sin\theta}{2\phi} (v_0^2 - 2H_0), \tag{15}$$

$$\frac{d\phi}{d\theta} = T \sin\theta \tag{16}$$

$$\frac{dR}{d\theta} = R \left(-\frac{S}{\sin\theta} - \frac{v_0^2 - 2H_0}{\phi} \frac{d\phi}{d\theta} + \frac{v_0^2 \cos\theta}{\sin\theta} \right) \tag{17}$$

where the auxiliary functions $S(\theta)$ and $T(\theta)$ are defined from equations (16) and (17).

The above equations are supplemented by four boundary conditions, two each on the axis and at the equatorial plane. On the axis $\theta = 0$, we demand

$$\phi \to 0 \quad \text{and} \quad S \equiv \sin\theta \left(-\frac{1}{R}\frac{dR}{d\theta} - \frac{v_0^2 - 2H_0}{\phi}\frac{d\phi}{d\theta} + \frac{v_0^2 \cos\theta}{\sin\theta} \right) \to 0. \tag{18}$$

The first condition means that the magnetic flux enclosed by the polar axis vanishes, and the second that the polar axis contains no line mass (see Li & Shu 1996 for a discussion). At the equatorial plane $\theta = \pi/2$, we impose the conditions

$$\frac{dR}{d\theta} = 0 \quad \text{and} \quad \frac{d\phi}{d\theta} = 0 \tag{19}$$

by symmetry. These translate to the requirements

$$S(\theta = \pi/2) = 0 \quad \text{and} \quad T(\theta = \pi/2) = 0. \tag{20}$$

Numerically, we integrate the set of first-order ODEs from small θ to larger values using a Runge-Kutta method. To initiate the integration, we use the following expansions at small angles that satisfy the boundary conditions near the polar axis listed in equation (18):

$$R = \theta^n (a_0 + a_2\theta^2 + c_0\theta^n + ...), \tag{21}$$

$$\phi = \theta^2 \left(b_0 - \frac{b_0}{12}\theta^2 + d_0\theta^n + ... \right), \tag{22}$$

$$S = \theta^2 \left[-(1 + H_0) + \frac{2a_0}{n+2}\theta^n + ... \right], \tag{23}$$

$$T = 2b_0 + \frac{a_0(v_0^2 - 2H_0)}{2nb_0}\theta^n + ..., \tag{24}$$

where $n = 4H_0 - v_0^2$ is the exponent of the dominant term in the expansion for the density $R(\theta)$. It reduces to the familiar form of $n = 4H_0$ for the nonrotating case (Li & Shu 1996).

The constants a_0 and b_0 are free parameters of the expansions. They are determined, for any given pair of H_0 and v_0, by shooting the solution towards the equator $\theta = \pi/2$ and matching the equatorial boundary conditions listed in equation (20). Other coefficients that appear in the expansions are related to these two parameters through

$$a_2 = \frac{a_0}{2}\left(1 - \frac{H_0}{3} + \frac{v_0^2}{12} + \frac{n}{4} \right), \tag{25}$$

$$d_0 = \frac{a_0(v_0^2 - 2H_0)}{2nb_0(n+2)}, \tag{26}$$

$$c_0 = \frac{a_0 d_0}{b_0}(2H_0 - v_0^2). \tag{27}$$

Equations (15) and (16) imply that the combination $H_0 - v_0^2/2$ is a measure of the angle-averaged support provided by magnetic fields in comparison with the level provided by thermal pressure. When this combination vanishes, the magnetic field is zero, and the pivotal configuration becomes a Hayashi-Toomre toroid. When this combination is greater than zero, we may introduce a better measure of magnetization, the dimensionless mass-to-flux ratio defined in equation (37) of Li & Shu (1996):

$$\lambda \equiv \int_0^{\pi/2} \frac{R(\theta)\sin(\theta)}{\phi(\theta)}\, d\theta. \tag{28}$$

A value of $\lambda = 1$ divides supercritical clouds from subcritical ones. Since our models have no bounding surface pressures, all cases encountered in this paper are supercritical, $\lambda > 1$. For example, the choice $(H_0, v_0) = (0.25, 0.25)$ produces the angular distribution functions displayed in Fig. 1. The integral of equation (28) then yields $\lambda = 4.61$, a case considered by observers to be magnetically "weak" (e.g., Crutcher 1999). However, far from satisfying the intuition that magnetic fields are therefore ignorable in the subsequent collapse, the relatively "weak" fields in the problem actually dominate many subsequent phenomena of crucial astrophysical interest – e.g., the formation of large pseudodisks, the transport of angular momentum, and the resulting size of centrifugally supported ("true") disks.

3. Collapse of Magnetized, Rotating Toroids

Numerically, we follow the inside-out collapse of the rotating toroid using Zeus2D (Stone & Norman 1992), which solves the ideal MHD equations in three dimensions with an axis of symmetry. Several modifications to the Zeus2D code were needed to follow the toroid collapse; these are discussed in Paper I for the nonrotating case. We refer the reader to that paper for details. The presence of rotation makes it necessary to consider the toroidal component of magnetic field, which is already included in Zeus2D.

3.1. Collapse of the $H_0 = 0.25$ and $v_0 = 0.25$ Toroid

To illustrate the general features of the collapse solutions, we first consider as a standard for comparison the case with $H_0 = 0.25$ and $v_0 = 0.25$. Toroids with different combinations of H_0 and v_0 will be discussed in the next subsection.

3.1.1. Central Mass Accretion

We first examine the time evolution of the mass accretion rate into the central cell (point mass), which is displayed in Fig. 2. To facilitate comparisons with observations, we have plotted the abscissa in physical time units, adopting a fiducial value for the isothermal sound speed of $a = 0.2$ km s^{-1}. The mass accretion rate into the central cell is plotted in units of $(1 + H_0)a^3/G$, and the asymptotic value, 0.80 is presumably the correct self-similar solution (for arbitrary values of a and physical times > 0) if one could rid the calculation of numerical artifices. Among such artifices is the possession of a strong initial peak in the accretion rate, reminiscent of the peak in the nonrotating case (Fig. 3d of Paper I) induced by an artificial point mass placed at the center to initiate the inside-out collapse. After a short period of adjustment, the central accretion rate quickly settles down to the more or less steady value of $\sim 0.80(1 + H_0)a^3/G$. The value is only slightly reduced (by $\sim 18\%$) from that of the corresponding nonrotating case (see Paper I). Evidently accretion into the central sink cell has not been significantly impeded by rotation.

3.1.2. Rotating Pseudodisk

The most prominent feature of the nonrotating collapse solution is the formation of a dense, flattened pseudodisk in the equatorial region (Paper I), which collapses radially towards the center. Inclusion of a modest amount of rotation does not significantly modify this basic density structure, as shown in Fig. 3. In the figure, the initial state is plotted, along with the collapse solution at $t = 2.5 \times 10^{12}$ seconds after the initiation of collapse when artifacts from the starting conditions have essentially disappeared (see Fig. 2). For the convenience of observers, we have again plotted the results in physical units using the canonical choice $a = 0.2$ km s^{-1} for low-mass cloud cores in Taurus. (Scalings to different values for a or to different times t occur by the rules given in eq. [3] of Paper I; these rules continue to hold even when u_φ and B_φ are nonzero.) The pseudodisk grows in the same way as it does in the nonrotating case. In fact, for the inner collapse region (say within a reduced radius of $x = r/at < 0.5$ or a dimensional radius of $r < 2.5 \times 10^{16}$ cm at a time $t = 2.5 \times 10^{12}$ s when $a = 0.2$ km s^{-1}), the density distributions of the rotating and nonrotating cases are practically indistinguishable from each other.

The main difference lies in the rotation of the pseudodisk, which is of course nonzero for the rotating case. In panel (c) of Fig. 3, we display contours of constant azimuthal speed. They show clearly that the pseudodisk, defined somewhat arbitrarily as the darkest region in the plot, has a significant rotation, with the (linear) rotational speed peaking in the middle section of the disk, in a "ridge" (or a "shell"in three dimensions) that extends from the disk

upwards into the envelope. The rotational speed has a maximum value $\sim 50\%$ above the sound speed. It falls off to subsonic values in regions both closer to the polar axis and further away. We note that, despite significant rotation, the motions inside the pseudodisk remain predominantly poloidal, as in the nonrotating case.

Another feature absent from the nonrotating case is the the twisting of magnetic field lines. In panel (d) of Fig. 3, we plot contours of constant field pitch-angle, defined as $\theta_{\rm t} = \tan^{-1}(B_\varphi/B_p)$, where B_φ and B_p are the toroidal and poloidal field strength. Clearly, (differential) rotation has distorted the initial, purely poloidal field configuration, although not by much. The maximum twist again occurs in a "ridge", roughly where the rotation is fastest, with a pitch angle of order 20°. In the polar region interior to the ridge, the plasma $\beta \ll 1$, and the field lines are essentially rigid against wrapping. Outside the ridge, the collapsing flow has yet to be spun up enough to wrap the field lines appreciably (even though the plasma β is greater than unity and would allow large twists).

A more graphical display of the 3D magnetic field is presented in Fig. 4. The view obtained at 60° inclination to the rotational and magnetic axis testifies to the relatively small amount of field wrapping that occurs in the problem because magnetic effects dominate those of rotation in the regions of interest. The pole-on view of the same magnetic field lines allows a clearer look at the top half of the twisted split-monopole configuration within the pseudodisk and permits a visualization of the magnetic torques ($\propto \varpi B_\varpi B_\varphi$, where $\varpi = r\sin\theta$ is the cylindrical radius) that lead to efficient angular momentum transfer and magnetic braking. The lack of significant field winding on scales of the outer pseudodisks and larger may explain why OH-maser polarization studies of magnetic-field directions in regions of massive star formation show surprising correlation with the large-scale magnetic field of the Milky Way Galaxy on a scale of at least 2 kpc (Reid & Silverstein 1990, Fish & Reid 2003). The implied accompanying loss of angular momentum in the gas during collapse may already have been detected in high-mass star-forming regions by Keto, Ho, & Reid (1987).

In the absence of angular momentum transport, we would have expected the formation of a rotationally supported disk with approximate size $0.25\, v_0^2\, at$, or $\sim 5 \times 10^{14}$ cm at the time shown in Fig. 3. No such disk has appeared in the actual calculation, perhaps because of the lack of adequate spatial resolution in the central regions, but more likely because of the efficiency of the magnetic braking, as we shall discuss in the next subsection.

One might also question whether the assumption of field freezing is likely to hold at small scales where densities are high and ionization fractions become very low. We address this practical question in § 4; here, we merely remark that a substantial layer of the pseudodisk is likely to remain suitably well coupled to magnetic fields almost right to the surface of the central protostar and makes equivocal any answer to whether or not one can expect the

formation of true Keplerian disks in the face of efficient magnetic braking.

3.1.3. Outflow, Magnetic Braking and Angular Momentum Redistribution

A somewhat unexpected feature of the collapse of the rotating toroid is the presence of an outflow region, part of which is already apparent in the upper-left corner of panel (b) of Fig. 3 from the velocity vectors. The highly distorted velocity contours (particularly that of $v = 1.0$) are another manifestation of its presence. In Fig. 5, we show the outflow more clearly over a larger region, including all four quadrants. The outflow has a relatively low speed, comparable to the sound speed a. It is thus unrelated to the famous bipolar molecular outflows of many CO observations. The same statement applies to the low-speed outflows obtained in Tomisaka's (1998, 2002) calculations, although Tomisaka expresses contrary sentiments. Nor are the motions to be confused with the fast-moving, hypersonic jet/wind that is thought to be driven from near the forming star (Königl & Pudritz 2000; Shu et al. 2000). Some shaping of such winds, if they start out in a wide-angle configuration (see Shang et al. 2002), might occur, if they, like their low-speed counterparts in Fig. 5, escape preferentially along the low-density, axial direction of the ambient medium. In any case, interaction between the fast-moving jet/wind of an embedded protostar with the transonic outflow/infalling envelope appears unavoidable, but we will postpone a treatment of this interaction to a future investigation.

The slow outflow is driven by magnetic braking. As collapse proceeds, matter in the magnetically dominated polar region (where the plasma $\beta < 1$) first slides along field lines towards the equatorial plane to create the dense, pseudodisk. The pseudodisk is not an equilibrium structure; its thermal and magnetic forces are too weak to balance the gravitational pull of the central object. As the material in the disk falls inward dynamically, it tends to spin up because of angular momentum conservation. However, the field lines threading the contracting pseudodisk also pass through the more slowly rotating envelope material higher up. The twisting of field lines in the pseudodisk generates a torsional Alfvén wave, which propagates away from the equatorial plane. The wave removes angular momentum from the pseudodisk and deposits it in a small fraction of the envelope material near the $\beta = 1$ line, which moves away as a low-speed wind. The outflow is concentrated in the "ridge" where the rotation is fastest and the field lines are most twisted (see panels [c] and [d] of Fig. 3). Closer to the polar axis, the plasma $\beta \ll 1$ and the wrapping of field lines unwinds almost instantaneously; further away, the field lines are not twisted enough to reverse the collapsing inflow. We will show below that, as the field strength increases, the slow outflow grows wider and faster.

The angular momentum redistribution due to magnetic braking is shown pictorially in Fig. 6. In the figure, angular momentum is depleted from the depressed, "valley" in the equatorial region due to collapse. In the absence of magnetic braking, all of the depleted angular momentum should be deposited in the pseudodisk, where the "mountain" in the figure is. Magnetic braking lowers the height of the "mountain" considerably, creating a "ridge" that runs more or less parallel to the polar axis. From the volumes beneath the "mountain" and the "ridge", we estimate that more than 90% of the angular momentum that would have accumulated in the pseudodisk is removed by magnetic braking in this particular case, although the fraction depends on the somewhat subjective choice of where the "ridge" ends and the "mountain" begins.

For ideal MHD, magnetic braking is very efficient. It removes most of the angular momentum of the infalling material before it enters the central cell. As a result, no centrifugally supported, thin disk that we could resolve numerically forms throughout the run of the simulation. We believe that even with increased numerical resolution a rotationally supported disk will not form in the ideal MHD limit under the isothermal assumption. The reason is that in any ideal, self-similar, calculation that has been carried out correctly, the origin must contain a point mass that grows linearly with time, and this mass must trap a magnetic flux with a dimensionless mass-to-flux given by the the original ratio λ. The trapped flux emanates from the center as a split monopole (Galli & Shu 1993b, Li & Shu 1996), which causes the infalling matter to become more magnetically dominant and slowly rotating as it approaches the origin. The reason for magnetic domination is obvious. That for slow rotation is less so, and can be shown mathematically as follows. Written in cylindrical coordinates, $(\varpi = r\sin\theta, \phi, z)$, the angular momentum equation for our problem reads

$$\frac{\partial}{\partial t}(\rho j) + \frac{1}{\varpi}\frac{\partial}{\partial \varpi}(\varpi \rho j u_{\varpi}) + \frac{\partial}{\partial z}(\rho j u_z) = \frac{1}{4\pi}\left[\frac{1}{\varpi}\frac{\partial}{\partial \varpi}(\varpi^2 B_{\varpi} B_{\varphi}) + \frac{\partial}{\partial z}(\varpi B_{\varphi} B_z)\right], \qquad (29)$$

where $j \equiv \varpi u_{\phi} \equiv \varpi^2 \Omega$ is the fluid specific angular momentum. If we integrate over a cylindrical volume of a small radius ϖ and infinite z height, and if we approximate the fluid distribution to be confined to an infinitesimally thin pseudodisk of surface density Σ, with $\rho(\varpi, z, t) = \Sigma(\varpi, t)\delta(z)$, we obtain

$$\frac{\partial J}{\partial t} + 2\pi\varpi\Sigma j u_{\varpi z=0} = 2\pi\varpi \int_{-\infty}^{+\infty} \frac{\varpi B_{\varpi} B_{\varphi}}{4\pi}\, dz, \qquad (30)$$

where

$$J(t) \equiv \int_0^{\varpi} \Sigma(\varpi, t) j_{z=0} 2\pi\varpi\, d\varpi. \qquad (31)$$

Equation (30) states that the time rate of change of J, the total fluid angular momentum contained within a circle of radius ϖ in the plane of the pseudodisk, plus the radial flux

of fluid angular momentum across the circumference $2\pi\varpi$ of the same circle, is equal to the torque exerted by the Maxwell stress acting across a cylindrical surface of midplane circumference $2\pi\varpi$ and infinite height in z. For B_ϖ satisfying a split monopole geometry, the torque on the right-hand side of equation (30) can be approximated as a negative constant times a representative mean value of $|B_\varphi|$ on the important part of this cylindrical surface.

Equation (11) states, on the other hand, that under the assumption of strict field freezing, azimuthal field B_φ is generated at a rate

$$\frac{\partial B_\varphi}{\partial t} = \varpi \left(B_\varpi \frac{\partial \Omega}{\partial \varpi} + B_z \frac{\partial \Omega}{\partial z} \right) . \tag{32}$$

If for small ϖ, Ω were to approach anything resembling a Keplerian field of differential rotation $\Omega \propto \varpi^{-3/2}$ in the presence of a point mass $M = \dot{M}t$ at the origin, then B_φ would be generated at a highly divergent rate $\propto \varpi^{-5/2}$. This behavior would lead to divergent negative torques on the right-hand side of equation (30) and rob the interior of angular momentum that it does not possess. The contradiction implies that centrifugally supported disks *cannot* form in the presence of frozen-in magnetic fields of typical interstellar origin if they are dragged into the central regions of a pseudodisk configuration. In such circumstances, the angular velocity Ω is more likely to reach a nearly constant value at small ϖ, saturating the spinup seen at large ϖ in the overall gravitational collapse. This combination of behaviors then explains why the *linear* velocity of rotation reaches a maximum value at some intermediate value of ϖ.

Since exterior gas must ultimately carry away the excess angular momentum transferred to them by magnetic torques, one way out of the dilemma posed above is to suppose that the magnetic fields on the outside can enforce strict isorotation on field lines, so that $\mathbf{B} \cdot \nabla\Omega = 0$. In practice this enforcement is possible only in a near-vacuum environment where Alfvén waves can propagate almost at infinite speed. In other words, we can expect braking to become less efficient once the toroidal Alfvén wave breaks out of the cloud boundary, a development neither allowed by our simulation protocol nor theoretically attractive as a general solution to the surprising dilemma of *too much* outward angular-momentum transport.

As we shall discuss in § 4, we believe a better alternative is ambipolar diffusion and/or magnetic reconnection to decouple eventually the pseudodisk from its attached magnetic field. This decoupling would diminish the braking efficiency and perhaps lead to a growing rotationally supported disk at some point during the gravitational collapse. The attractiveness of this proposal lies in the unified possibility of resolving two problems of long-standing in star formation without invoking additional physical processes: the loss of the magnetic flux associated with trapped interstellar fields, and the appropriate outward transport of

angular momentum in disks and pseudodisks. To wit, an unmagnetized, rotating cloud will not collapse directly to a central point-like mass, whereas an ideally magnetized, nonrotating cloud can collapse to a central point-like mass without a rotationally supported disk. With more realistic physics (see § 4.1), a magnetized, rotating cloud may collapse to a protostar while forming a Keplerian disk that could eventually produce a planetary system. Alternatively, if the disk or pseudodisk becomes sufficiently massive in the process, nonaxisymmetric gravitational instabilities may take over to yield binary and/or multiple star systems (see, e.g., the speculations of Galli et al. 2001).

3.2. Effects of Rotational Speed on Collapse Solution

We now explore, for a fixed value $H_0 = 0.25$ for the over-density parameter, a range of values for the dimensionless rotation rate: $v_0 = 0, 0.125, 0.25$ and 0.5. The corresponding dimensionless mass-to-flux ratios λ of the sequence are 4.51, 4.61, 4.94, and 7.15. Thus, the sequence not only represents the effects of increasing rates of rotation on the collapse, but also those of a decreasing magnetic field (both as measured against the support provided by thermal pressure). The self-similar results, all obtained by running the simulations long enough to eliminate unwanted transients, are shown in Fig. 7.

To begin the discussion, we note that rotation has only a modest effect on the density distribution of the collapse solution. The pseudodisk is slightly thicker for a faster rotation, partially because the infall is retarded more by rotation, and partially because of a more vigorous outflow (still very slow by bipolar outflow standards, not to mention stellar jets), which lifts up some of the disk material (see panel [d]). The increasing strength of outflow as v_0 increases is most evident in the shape of the constant (total) velocity contour of $v = 1$, which gets more distorted for a larger v_0. The distortion comes mostly from the toroidal component of the velocity, which can be close to the sound speed or larger in the magneto-rotationally driven outflow. An interesting feature, related to the strength of the outflow and the strength of the pre-collapse magnetic field, is that the magnetically dominated region enclosed by the $\beta = 1$ line shrinks as v_0 increases. This effect is seen most clearly in the fastest rotating, most weakly magnetized $v_0 = 0.5$ case, where the enhanced density in the outflow has apparently pushed the $\beta = 1$ line close to the polar axis. Note also the pronounced distortions of the density contours and field lines caused by the outflow in this case.

Rotation decreases somewhat the rate of mass accretion onto the central point mass, a trend also present in the calculations of Tomisaka (2002) and Krasnopolsky & Königl (2002). In steady state after the initial transient peak, the accretion rate is reduced, respectively, by

about 14%, 18% and 33% for $v_0 = 0.125, 0.25$ and 0.5, in comparison with the nonrotating case $v_0 = 0$. The reduction may be due to a combination of slower infall and mass removal in the outflow. However, the numerical outward diffusion of magnetic field exacerbated by artificial viscosity mediating shock waves at the boundaries of the central cell could also help to lower effective mass-accretion rates. In any case, for values of v_0 approaching the upper limit $\sqrt{2H_0}$ that would make the associated magnetic field in the model go to zero, we expect the central mass accretion rate to go to zero in any axisymmetric calculation that also suppresses gravitational torques. By explicit calculation, we verified the formal vanishing of $\dot{M}$ into the central cell for nonmagnetic calculations in which v_0 had a large enough value (e.g., 0.5) to allow the numerical resolution of a centrifugally supported disk.

3.3. Effects of Magnetic Field Strength on Collapse Solution

For a nonmagnetic Toomre-Hayashi toroid, $H_0 = v_0^2/2$. The axisymmetric collapse of such a toroid should not directly produce a point mass at the center in principle. In practice, the numerical grid is finite, and the central cell will experience some mass accretion, particularly when the rotational speed v_0 is small. Sooner or later, the numerical artifacts disappear from our simulations as the outward expansion of infall occupies more and more computational cells. The "central" accretion diminishes drastically, when most of the infall material lands on a spatially resolved, rotationally supported, disk of approximate size $x_d \approx 0.25 v_0^2$, in dimensionless units of ϖ/at. In an axisymmetric simulation, the accreted material simply accumulates in the disk because all processes of angular momentum removal or redistribution are suppressed in the absence of any magnetic and gravitational torques. Eventually the disks become sufficiently massive that they are gravitationally unstable to axisymmetric transformation into rings (Toomre's 1964 instability; see also Goldreich & Lynden-Bell 1965), a condition that plagues the long-time behavior of some of our computed nonmagnetic results. In a perfect self-similar collapse simulation, some inner part of the disk would always be unstable by Toomre's criterion, but the difficulty does not manifest itself practically until the calculation has proceeded long enough for these regions to become sufficiently spatially resolved in a finite-difference scheme.

The magnetized, rotating collapse is qualitatively different due to magnetic braking. Angular momentum removal, particularly in the magnetically dominated region close to the origin (where $\beta < 1$), allows infall material to accrete all the way onto the central cell, provided that ideal MHD holds.

To begin our exploration of these effects of magnetic fields, we fix the rotational speed v_0 at the fiducial value of 0.25, and consider four different values of $H_0 = 0.03125$ ($\lambda = \infty$),

0.125 ($\lambda = 10.0$), 0.25 ($\lambda = 4.94$), and 0.5 ($\lambda = 2.77$). The $H_0 = 0.03125$ case satisfies the nonmagnetic relation $H_0 = v_0^2/2$, so the mass-to-flux ratio is infinite. This rotating toroid is initially close to being spherical, containing only $v_0^2/2 \approx 3\%$ more mass than a singular isothermal sphere. It has a ratio of rotational to gravitational energy of $\sim (v_0/2)^2 = 1.56\%$, which is typical of molecular cloud cores (Goodman et al. 1993). Its collapse is followed with Zeus2D, with the magnetic field turned off. The results are shown in panel (a) of Fig. 8. The collapse solution resembles that of the singular isothermal sphere shown in Fig. 6a of Paper I, except very close to the origin, where flattening of the mass distribution because of rotation becomes more prominent. The expected size of the rotationally supported disk, $x_d \equiv \varpi_d/at \approx 0.016$ is too small to be resolved by our grid, or the scale of the figure, in this particular example. However, by keeping track of the mass and angular momentum that flowed into the central cell, we verified that angular momentum conservation holds to high accuracy in our modified version of the Zeus2D code.

As H_0 increases well beyond $v_0^2/2 = 0.03125$, most of the extra mass over the singular isothermal sphere is supported by magnetic fields rather than rotation. This is the case for $H_0 = 0.125, 0.25$ and 0.5, whose collapse solutions are displayed in panels (b)-(d) of Fig. 8. These panels are to be compared with panels (b)-(d) of Fig. 6 of Paper I, where the corresponding nonrotating collapse solutions are plotted. In all cases, the density distribution shows a prominent pseudodisk, and the velocity field contains a slow outflow component. The former is basically a magnetic structure; it increases in size and becomes more flattened as the field strength (or H_0) increases, as expected. The latter is due to a combination of magnetic fields and rotation. We find that, for a given v_0, as the field strength increases, the outflow becomes faster and wider. It also starts at a larger height above the pseudodisk, most likely as a result of a faster propagation speed for the torsional Alfvén wave in the more strongly magnetized case.

In each of the three magnetized cases, the slow outflow removes the bulk of the angular momentum originally associated with the accumulated mass in the central cell. Determining the exact fraction of the angular momentum removed is somewhat uncertain. As a rough estimate, we divided the average specific angular momentum of the central-cell mass by that in the nonmagnetic case. The ratio typically turns out to be of order 10^{-3} or smaller in our best resolved examples, and smaller than 0.1 in almost all cases. But in some sense the exercise is pointless, since in a perfectly resolved calculation, where the central object becomes a point mass, its angular momentum has to go to zero. The physically meaningful number is not how much angular momentum has to be transferred for matter to reach the center, but what is the mass-accretion rate achieved in accomplishing this feat, with and without magnetization in the problem. Complicating a definitive answer to the latter question is the numerical instability described already in Paper I that leads to oscillations of

the magnetic field configuration as it becomes severely pinched and relaxes by numerically unpinching. Such oscillations become more severe at late times in the simulation (defined by when the innermost parts of the simulation become well resolved), and interfere thus in a fundamental way with a determination of the time-steady value of the central $\dot{M}$.

In the interim, we can examine the effects of magnetic braking on rotation a little more directly. In Fig. 9, we plot the contours of constant rotational speed for the nonmagnetic and magnetic cases. Note that the nonmagnetic cloud rotates fastest on small scales, and this rotation is braked significantly in all of the three magnetized cases, with the pseudodisk in the most strongly magnetized case rotating most slowly, as expected. A feature common to all magnetized cases is the strong differential rotation in and around the pseudodisk, with the rotational speed peaking in the middle sector where the outflowing "ridge" originates. The much smaller rotational speed in the region close to the axis (interior to the ridge) compared with that in the nonmagnetic case provides clear evidence that most of angular momentum is indeed stripped before mass enters the central cell.

4. Discussion and Conclusion

4.1. Magnetic Braking and Keplerian Disk Formation

Formation of centrifugally supported circumstellar disks is a central problem in star and planet formation. The initial distribution of angular momentum in the dense core, which collapses to form the star and disk, and the angular momentum redistribution during the collapse and disk accretion both affect the final outcome. We have shown that almost all of the core angular momentum can be removed in a low-speed outflow driven by magnetic braking during the collapse, provided that (1) the core is significantly magnetized and (2) the ideal MHD approximation holds. We now examine these two conditions from a practical point of view.

The degree of magnetization of dense cores of molecular clouds prior to collapse is somewhat uncertain. In the standard scenario for isolated low-mass star formation (Shu et al. 1997; Mouschovias & Ciolek 1999), the cores are envisioned to form out of a magnetically subcritical background cloud (bounded at its surface by significant thermal or ram or turbulent pressure), with the evolution driven by ambipolar diffusion. The cores remain well magnetized, even during the supercritical phase of evolution, when their dimensionless mass-to-flux ratio λ is about 2 (Basu & Mouschovias 1994; Nakamura & Li 2003). This ratio, corresponding to $H_0 - v_0^2/2 \approx 0.5$ (Li & Shu 1996, this paper), is consistent with the field strength obtained for the well studied cores L1544 (Crutcher & Troland 2000) and

B1 (Goodman et al. 1989) from Zeeman measurements, after likely geometric corrections (Crutcher et al. 1994; Shu et al. 1999; Ciolek & Basu 2000). Polarization has been detected in the dust continuum emission from a number of cores (e.g., Ward-Thompson et al. 2000; Matthews & Wilson 2002), which also points to a significant degree of magnetization. In addition, the cores are known to be elongated in general, with a typical aspect ratio of 2:1 (Myers et al. 1991); the elongation is too large to be induced by rotation, and is consistent with the presence of a dynamically important magnetic field (Li & Shu 1996). Even if the molecular clouds are magnetically supercritical to begin with and cores form in them dynamically, it would still be difficult to avoid having an $H_0 - v_0^2/2$ at least as high as 0.2 to 0.3, which corresponds to a weak field of ~ 3 μG threading a slab of interstellar medium of $A_{\rm V} = 1$. Based on these arguments, we believe that the dense cores formed in present-day star-forming clouds should trap enough magnetic flux for magnetic braking to operate efficiently during gravitational collapse, as long as the field remains well coupled to the bulk of the neutral core matter.

Good coupling between the magnetic fields and neutral matter is maintained through collisions with ions in relatively low-density regions of a dark, molecular cloud core. In such regions, the primary source of ionization, and the time scale for ambipolar diffusion is typically an order of magnitude longer than the dynamic time scale[1], which means that there is little time for magnetic flux to be redistributed in a dynamically collapsing flow. Thus, ideal MHD is a reasonable first approximation in collapse calculations. Nishi et al. (1991; see also Desch & Mouschovias 2001) claim that good coupling is lost above a volume density of order 10^{11} cm^{-3}. Magnetic decoupling occurs for densities higher than this critical value, which reduces the efficiency of the magnetic braking. The decoupling density well exceeds the density in most of the pseudodisk, which is typically less than $\sim 10^7$ cm^{-3} (see the density contours in Fig. 3 for an example), except in one or two zones right next to the central cell. Therefore, most of the angular momentum of the collapsing core material is already removed by magnetic braking before the braking is rendered ineffective by decoupling.

Let us now examine the supposition that the gas volume density will eventually exceed the critical value for decoupling. While true in rotationally supported protoplanetary disks with similar physical properties to the so-called "minimum solar nebula," it is not necessarily the case for the dynamically collapsing pseudodisks, whose surface densities are much lower and provide less shielding against cosmic ray ionization. It is an easy matter to estimate the surface density Σ of a flattened configuration accreting axisymmertically in quasi-steady

[1]In the more turbulent, lower density envelope surrounding a dense core, the time scale for ambipolar diffusion can be shortened considerably through field fluctuations (Fatuzzo & Adams 2002). The faster ambipolar diffusion may affect the angular momentum evolution during the early phase of core formation.

state $\dot{M}$ at radial speeds that approach free-fall values $\sqrt{2GM/\varpi}$ onto a central mass M:

$$\Sigma = \frac{\dot{M}}{2\pi\varpi\sqrt{2GM/\varpi}} = 0.16 \text{ g cm}^{-2} \left(\frac{\dot{M}}{10^{-6}\ M_\odot \text{yr}^{-1}}\right) \left(\frac{M\ \varpi}{M_\odot\ \text{AU}}\right)^{-1/2} . \qquad (33)$$

Within a factor of 2 or so, the inner regions of pseudodisks obtained by numerical simulation in this paper satisfy the estimate of equation (33).

Galactic cosmic rays can keep a layer with a surface density of about 100 g cm^{-2} sufficiently ionized as to couple well to magnetic fields (Nishi et al. 1991). Thus, in the absence of a magnetized YSO wind or jet that can sweep out cosmic rays before they penetrate pseudodisks, Galactic cosmic rays will make a pseudodisk with a surface density profile given by equation (33) sufficiently well-ionized all the way to the surface of a protostar with characteristic radius $\sim 10^{-2}$ AU. Even after a YSO jet or wind turns on, if the event is accompanied by stellar magnetic activity and the emission of X-rays, the observed levels of X-rays in low-mass protostars are sufficient to keep a layer with the surface-density profile of equation (33) marginally well-coupled (Glassgold, Najita, & Igea 1997).

Why then, should centrifugally supported disk ever arise? Because the coupling to magnetic fields in the pseudodisks, while good, is not perfect. Nonideal MHD effects of two types have been described in the literature that can substantially modify the discussions considered so far in this paper.

Li & McKee (1996) focused on slippage of magnetic flux in the radial direction by the effects of ambipolar diffusion. They proposed that the magnetic flux decoupled this way from the mass that enters the star can drive a hydromagnetic shock against the collapsing inflow. Behind the shock, the accretion flow can be slowed down by a large factor, and become magnetically dominated. It is conceivable that magnetic braking would still remove a large fraction of the remaining angular momentum in the slowly-contracting post-shock region (Krasnopolsky & Königl 2002).

Galli & Shu (1993b) focused on the vertical stratification produced by the highly pinched magnetic field in the pseudodisk as a condition whereby magnetic flux can be lost by reconnection. As we also noted in this paper and paper I, infall in the pseudodisk tends to produce a split-monopole geometry with reversed poloidal fields across the midplane. In an ideal MHD calculation, the reversed magnetic fields across the midplane are supported by current sheets. In reality, the large electric current density near the midplane will dissipate by the presence of nonzero electrical resistivity. The dissipation of these currents corresponds to annihilation of the reversed fields above and below the midplane. The higher magnetic pressures of the surrounding regions will then press toward the middle, leading to further field annihilation. Except for the continued introduction of new interstellar flux by infall

into the pseudodisk, the entire magnetic flux threading the pseudodisk could eventually be lost by this reconnection process.

In quasi-steady state, we therefore expect a "sandwich-like" structure to develop. The "bread" of the sandwich is the well-coupled, magnetized, regions where angular momentum can be removed at a sufficient pace as to allow the matter to spiral essentially unimpeded at dynamical rates toward the central protostar. This bread is the radially inward extension of the original pseudodisk, and it may already have been detected in the case of IRS L1489 by the observations of Boogert, Hogerheijde, & Blake (2002). The "meat" of the sandwich is the part which is sufficiently shielded by the bread against external ionizing radiation as to become essentially decoupled from any magnetic fields. This decoupling causes eventual spinup of the inwardly spiraling material, because of the lack of magnetic braking, and the eventual formation of a centrifugally supported disk. This "true" disk is bounded above and below by the dynamically infalling remnant of the pseudodisk. How massive the meat becomes relative to the bread is, at this point, entirely a matter of speculation. It could vary considerably between regions of isolated star formation, such as Taurus-Auriga, and regions of crowded star formation, such as Orion, because of the difference of ionizing radiation (particulates and photons) associated with star-birth activity.

Like many examples in astrophysics, moreover, such as the Sun or other magnetically active stars, the reconnection process may occur not quiescently but explosively and intermittently in flares. It is interesting to speculate whether such intermittent behavior has anything to do with FU Orionis outbursts. Other effects may enter to further complicate the situation. The flow could become turbulent because of Kelvin-Helmholtz instabilities that arise from the velocity shear between the bread and meat parts of the sandwich, or because of interchange instabilities in 3D that manifest themselves in the pinched magnetic configuration of the split-monopole. Under laminar conditions, resistive effects become important in the same density regime where ambipolar diffusion becomes competitive with the dynamics (Nishi et al. 1991), so a combination of the effects discussed by Galli & Shu (1993b) and Li & McKee (1996) may be operative. All these effects operating together in lightly ionized media, under turbulent conditions, may considerably increase the size scales over which nonideal effects must be considered (Zweibel & Brandenburg 1997a, b). Challenging nonideal 3D simulations with adaptive mesh refinement may be needed to quantify such possibilities.

4.2. Comparison with Previous Work

Magnetic braking in star formation has been studied previously by many authors, in connection with the long-standing "angular momentum problem". Most of the early studies were concerned with the relatively low-density, initial stage of star formation using semi-analytic treatments (e.g., Mestel & Paris 1984; Nakano 1989; see Mouschovias 1990 for a review). Recent numerical calculations have extended the treatment to higher densities associated with the runaway core contraction either prior to star formation (Basu & Mouschovias 1994) or slightly beyond the formation of a central object (Tomisaka 2002). These calculations showed that, during the short runaway phase when the central density increases by several orders of magnitude, the angular momentum is nearly conserved, because the density increase involves little positional change of fluid elements in both radial and azimuthal directions (and thus little pinching and twisting of field lines). Our work deals exclusively with magnetic braking in the infall or accretion phase, *after* the formation of a compact central object. One may naively think that, once a molecular-cloud core starts to collapse dynamically, there should be little time for magnetic braking to operate. And yet we find that the bulk of the angular momentum, if not the total, can be removed during the dynamical collapse, even with a magnetic field of relatively moderate strength. Why is there this difference between previous expectations and current calculations?

There are two key ingredients behind the efficient braking during the accretion phase: (1) the domination of magnetic energy over the rotational energy, and (2) the distinct geometry of the magnetic field. The foot points of the magnetic field lines associated with the matter already landed on the central object are pinned near the origin by accretion, creating a split monopole for the magnetic geometry (see Fig. 3). The split-monopole field lines push on the field lines outside (see also Li & Shu 1997), bending them into an hour-glass shape that is conducive to efficient magnetic braking. The enhancement comes from both the greater field strengths due to pinching and the radial fan-out (as opposed to vertical collimation) which lengthens the level arm for magnetic braking. These two effects are not taken into account in previous simple estimates. They are analogous to magneto-centrifugally driven winds (Königl & Pudritz 2000; Shu et al. 2000). Indeed, the slowly moving outflow we find in the collapse solution is fundamentally similar to these winds, except for scale and for the ultimate origin of the field (interstellar, disk dynamo, or stellar dynamo).

Magneto-rotationally driven outflows were also found in the collapse calculations of Tomisaka (1998, 2002). These calculations start from infinitely long cylinders with magnetic field lines parallel to the axis. The magnetized cylinder is induced to break up into dense cores by a sinusoidal density perturbation along its length. The subsequent core evolution prior to the formation of a central object is more dynamic than that driven by ambipolar

diffusion. It produces a pivotal state at time $t = 0$ (when a *hydrostatic* core starts to form in the calculation) that differs substantially from the singular toroids that we adopted based on ambipolar diffusion calculations. Nevertheless, soon after the appearance of the hydrostatic core, an outflow develops, which Tomisaka attributed to core formation. A more precise cause for the outflow, we believe, is the trapping of a finite amount of magnetic flux (rather than mass) in a small (core) region, which gives rise to the central magnetic monopole responsible for the pinched magnetic geometry that is conducive to outflow driving. For numerical reasons, Tomisaka's calculations were stopped a short time into the accretion phase, typically 4×10^{-3} times the free-fall time at the center of the initial cylinder beyond the moment of hydrostatic core formation (t=0). During this brief period of time, the outflow appears to have removed most of the angular momentum of the material close to the origin (Tomisaka 2000). In particular, no rotationally supported disk is able to form, consistent with our findings which, because of their self-similar nature, apply to all times $t > 0$.

Formation of rotationally supported disks during the collapse of dense cores formed in strongly magnetized molecular clouds was recently examined by Krasnopolsky & Königl (2002) under thin-disk approximation. The material in the disk is connected through field lines to an external medium, which brakes the disk rotation with a parameterized efficiency. They find that, in the ideal MHD limit, a rotationally supported disk can form, provided that the braking efficiency is low enough (see their Fig. 3). If the braking is more efficient, the disk angular momentum can be radiated away completely, as shown in their Fig. 6. Our calculations and those of Tomisaka (1998, 2002), which treat the dynamics of the material above and below the disk self-consistently, suggest that the braking efficiency is high enough to prevent the rotationally supported disk from forming in a strongly magnetized core, as long as ideal MHD holds. In the presence of ambipolar diffusion, Krasnopolsky & Königl (2002) find that the bulk neutral material can retain a small rotation even in the strong braking case, because the neutral component must rotate relative to the charged component in order to feel the magnetic braking torque (see their Fig. 10). Whether the residual angular momentum is large enough in realistic situations to form a rotationally supported disk well outside the forming star remains to be seen.

To conclude this subsection, we note an interesting feature of regarding numerical errors, which are always present, of course, in any simulation. Simulations of self-similar configurations such as ours confer the advantage that although one does not know (in analytically intractable situations) what the exact details of the solution should be, one does know from dimensional considerations how each quantity should scale. This knowledge provides a powerful check on the present simulations, and therefore we have a good handle on the numerical reliability of the results quoted in this paper.

4.3. Observational Implications: The Case of IRAM 04191

Rotation introduces a new feature into our collapse solution - the slow outflow (see also Tomisaka 1998, 2002). Despite its crucial role in angular momentum redistribution, this outflow is unlikely to be observed soon: it is too easily masked by the faster-moving bipolar molecular outflows driven by a jet/wind from near the central object. Another prominent feature of the collapse solution – the flattened, high-density pseudodisk in the equatorial region – should be less affected by the bipolar outflow. Indeed, there are many examples of dense structures surrounding deeply embedded YSOs that are elongated perpendicular to the outflows. They can be plausibly interpreted as the pseudodisks formed during the collapse of magnetized toroids or, on a larger scale, the more static toroids themselves, although detailed kinematic studies and direct measurements of the strength and morphology of magnetic fields are needed to strengthen the case. The best studied circumstellar structure of this type is perhaps the one around the source IRAM 04191 (Belloche et al. 2002), which we discuss in some depth below.

IRAM 04191 is a low-luminosity ($L_{\rm bol} \sim 0.15 L_\odot$) protostar in the nearby Taurus molecular cloud, surrounded by a massive envelope ($M_{\rm env} \sim 1.5 M_\odot$; André, Motte, & Bacmann 1999). This Class 0 source drives a well-developed molecular outflow, as all Class 0 sources do. Perpendicular to the outflow lies a flattened structure that is mapped in both dust continuum and several molecular lines (Belloche et al. 2002). The line study revealed that the flattened structure is infalling at a velocity between half and one isothermal sound speed, with a substantial amount of rotation. The (linear) rotational speed increases from $\sim 0.2\ a$ at a radius of $\sim 11,000$ AU to $\sim a$ at $\sim 3,500$ AU, where $a \approx 0.2$ km s^{-1} is the isothermal sound speed at 10 K (see Fig. 12c of Belloche et al. 2002). We identify the increase in rotational speed with the spinup in the outer part of the pseudodisk as a result of radial contraction under the approximate conservation of specific angular momentum, before significant magnetic braking sets in. In our model, the rotational speed peaks at some radius, and then decreases inward in a region of strongly pinched magnetic field that efficiently removes the angular momentum of the accreting flow, as shown in Fig. 3c. If the flattened structure of IRAM 04191 is indeed a pseudodisk, then its rotational speed should decrease inward inside $\sim$ 3,500 AU according to our model. This is consistent with, but not required by, the available spectral data, particularly the "S"-shaped position-velocity diagrams of several molecular species. Higher resolution observations are needed to test the model. The test may be hampered by the freeze-out of molecules onto dust grains in the high-density region near the protostar, as evidenced by the "hole" in the NH_3 distribution around this source (Wootten et al. 2003).

Interpreting the flattened structure of IRAM 04191 strictly in terms of the models of

this paper is not without difficulties. In the fiducial case where $v_0 = 0.25$ (comparable to the 0.2 a seen at 11,000 AU in IRAM 04191), the rotational speed achieves a peak near the observed value $\sim a$ at a reduced radius of $x_{\rm p} \sim 0.25$. If this corresponds to the radius of $3,500$ AU for IRAM 04191, then the collapse would have been initiated $\sim 3.3 \times 10^5$ yrs ago, and the central star would have a mass of $\sim 0.8 M_\odot$. But the dynamical time for the molecular outflow of IRAM 04191 is only $\sim 8 \times 10^3$ yrs, much shorter than the above estimate. The low luminosity 0.15 $L_\odot$ of the central source also suggests a fairly small mass for the central star, accreting gas at not much higher than the standard rates for Taurus (see, e.g., Adams, Lada, & Shu 1987).

A flawed way to reconcile theory and observation, within the context of quasi-steady flow, is to postulate a significant temporal offset between the pivotal instant $t = 0$ and the appearance of a powerful outflow in the system. Such an offset requires, for example, some way to store infalling material (from a pseudodisk) in a rotationally supported disk without producing either much accretion luminosity or an outflow for a duration approaching 10^5 yr. This task is not easy to do without inducing fierce nonaxisymmetric gravitational instabilities that would undermine the assumption of little mass accretion into the central regions. Moreover, the observational limit claimed for the mass or size of any disk in IRAM 04191 is less than $\sim 10^{-3}$ $M_\odot$ or 10 AU. Efficient magnetic braking has evidently prevented a more massive/larger disk from forming close to the star, and such braking works against the idea of appreciable mass storage in a disk.

A better solution might be to suppose that, in addition to an offset between the pivotal instant and the onset of a wind, accretion onto the central source is time-variable, with FU Orionis outbursts punctuating quiescent periods of relative calm (Hartmann, Kenyon & Hartigan 1993). In such a picture, IRAM 04191 has just recently experienced such an outburst (accounting for the associated powerful molecular outflow) and has now faded considerably in its accretion luminosity (accounting for the low luminosity currently). Oscillatory inflow into the central regions in the presence of steady infall from the pseudodisk is a common bane of our simulations (see the discussion in Paper I). It remains to be seen whether the numerical artifact of field pinching and unpinching observed in the simulations might not have their physical analogues in more realistic calculations performed with nonideal MHD.

Another plausible option invokes a pre-existing contracting and rotating toroid to explain the observations of the regions at a few thousand AU and beyond. Subsonic cloud contraction prior to the formation of a formal density singularity for $t < 0$ is consistent with the observed motions in both IRAM 04191 and the well-studied starless core L1544 (Tafalla et al. 1998). As discussed already in Paper I, subsonic contraction of the requisite magnitude might be initiated by the dissipation of turbulent support in dense molecular-cloud

cores (Myers 1999) or resulted from ambipolar diffusion (e.g., Ciolek & Basu 2000). We have performed simulations of the fiducial (rotating and magnetized) case with an initial uniform radial inflow u_r equal to half the sound speed a. As we found in Paper I for the example without rotation, the results look like the configuration started without initial radial motion, except that the density profiles next to the axis are partially filled in by the additional inflow and the central accretion rate is increased by about a factor of 2.

4.4. Conclusion

To summarize, we have studied numerically the inside-out collapse of rotating, magnetized singular isothermal toroids. We find that a pseudodisk forms, just as in the nonrotating case, through which most of the core material is accreted. The pinched magnetic field in the pseudodisk removes most of the angular momentum of the accreted matter, and deposits it in a low-speed wind. The efficient magnetic braking during the protostellar accretion phase has important implications for the formation of rotationally supported disks that need to be pursued with nonideal MHD calculations.

The complementary side to this phenomenon is the discovery of an extremely simple and efficient mechanism of angular momentum transport that allows direct accretion of extended rotating material onto relatively compact objects without the necessary concomitant formation of a standard viscous accretion disk. Whether this mechanism has anything to do, for example, with the mini-spiral that seems to be feeding ionized gas, with low radiative efficiency, into the massive black hole at the center of our own Galaxy (Lo & Claussen 1983) remains to be seen. We have speculated in this paper that the process, with the inclusion of nonideal MHD effects, opens new vistas by which the two classical conundrums of star formation discussed long ago by Mestel and Spitzer – the angular-momentum problem and the magnetic-flux problem - might be resolved, perhaps simultaneously, in the disks and pseudodisks surrounding newly formed stars.

We thank A. Königl and R. Krasnopolsky for useful correspondence. Support for this work was provided in Taiwan in part by grants from Academia Sinica and the National Science Council, and in the United States by grants from the National Science Foundation and NASA.

REFERENCES

Adams, F. C., Lada, C. J. & Shu, F. H. 1987, ApJ, 312, 788

Allen, T., Shu, F. H. & Li, Z.-Y. 2003, ApJ, submitted (Paper I)

André, P., Motte, F. & Bacmann, A. 1999, ApJ, 513, L57

Basu, S. & Mouschovias, T. 1994, ApJ, 432, 720

Baureis, P., Ebert, R., & Schmitz, F 1989, AA, 225, 405

Belloche, André, P., Despois, D., & Blinder, S. 2002, AA, 393, 927

Boogert, A. C. A., Hogerheijde, M. R., & Blake, G. A. 2002, ApJ, 568, 761

Cai, M. J. & Shu, F. H. 2002, ApJ, 567, 477

Cai, M. J. & Shu, F. H. 2003, ApJ, 583, 391

Ciolek, G. E. & Basu, S. 2000, ApJ, 529, 925

Crutcher, R. M. 1999, ApJ, 520, 706

Crutcher, R. M., Mouschovias, T. Ch., Troland, T. H. & Ciolek, G. E. 1994, 427, 839

Crutcher, R. M. & Troland, T. H. 2000, ApJ, 537, L139

Desch, S. J, & Mouschovias, T. 2001, ApJ, 550, 314

Ferraro, V. C. A. 1937, MNRAS, 97, 458

Fiege, J. D., & Pudritz, R. E. 2000, 534, 291

Fish, V. L. & Reid, M. J. 2003, ApJ, submitted

Futuzzo, M. & Adams, F. C 2002, ApJ, 570, 210

Galli, D. & Shu, F. H. 1993a, ApJ, 417, 220

Galli, D. & Shu, F. H. 1993a, ApJ, 417, 243

Galli, D., Shu, F. H., Laughlin, G. & Lizano, S. 2001, ApJ, 551, 367

Glassgold, A. E., Najita, J., & Igea, J. 1997, ApJ, 480, 344

Goldreich, P. & Lynden-Bell, D. 1965, MNRAS, 130, 97

Goodman, A. A., Crutcher, R. M., Heiles, C., Myers, P. C., & Troland, T. H. 1989, ApJ, 338, L61

Goodman, A. A., Benson, P. J., Fuller, G. A. & Myers, P. C. 1993, ApJ, 406, 528

Hayashi, C., Narita, S., & Miyama, S. M. 1982, Prog. Theor. Phys., 68, 1949

Hartmann, L., Kenyon, S. J. & Hartigan, P. 1993, in Protostars and Planets III, ed. E. H. Levy & J. I. Lunine (Arizona: University of Arizona Press), p497

Königl, A., & Pudritz, R. E. 2000, in Protostars and Planets IV, ed. V. Mannings, A. Boss, and S. Russell (Arizona: University of Arizona Press), p759.

Keto, E. R., Ho, P. T. P., & Reid, M. J. 1987, ApJ, 923, L117

Krasnopolsky, R. & Königl, A. 2002, ApJ, 580, 987

Li, Z.-Y., & McKee, C. F. 1996, ApJ, 464, 373

Li, Z.-Y. & Shu, F. H. 1996, ApJ, 472, 211

Li, Z.-Y. & Shu, F. H. 1997, ApJ, 475, 237

Lizano, S. & Shu, F. H. 1989, ApJ, 342, 834

Lo, K. Y. & Claussen M. J. 1983, Nature, 306, 647.

Matthews, B. C. & Wilson, C. D. 2002, ApJ, 574, 822

Mestel, L. 1985, in Protostars and Planets II, eds. D. C. Black & M. S. Matthews (Tucson: University of Arizona Press), p. 320

Mestel, L. & Paris, R. B. 1984, AA, 136, 98

Mouschovias, T. Ch. 1990, in The Physics of Star Formation and Early Stellar Evolution, eds. C. J. Lada & N. D. Kylafis (Dordrecht: Kluwer), 449

Mouschovias, T. Ch. & Ciolek, G. 1999, in The Origins of Stars and Planetary Systems, ed. C. Lada & N. Kylafis (Dordrecht: Kluwer), p. 305

Myers, P. 1995, in Molecular CLouds and Star Formation, eds. C. Yuan & J. You (Singapore: World Scientific), p.47

Myers, P. C. 1999, NATO ASIC Proc. 540: The Origin of Stars and Planetary Systems, 67

Myers, P. C., Fuller, G. A., Goodman, A. A., & Benson, P. J. 1991, ApJ, 376, 561

Nakamura, F. & Li, Z.-Y. 2003, ApJ, in press

Nakano, T. 1989, MNRAS, 241, 495

Nishi, R., Nakano, T., & Umebayashi, T. 1991, ApJ, 368, 181

Reid, M. J. & Silverstein, E. M. 1990, ApJ, 361, 483

Simon, M., Ghez, A. M., Leinert, Ch., et al. 1995, ApJ, 443, 625

Shu, F. H., Adams, F. C., & Lizano, S. 1987, ARA&A, 25, 23

Shu, F. H., Allen, A., Shang, H., Ostriker, E. C., & Li, Z. Y. 1999, in *The Origin of Stars and Planetary Systems*, ed. C. Lada & N. Kylafis (Dordrecht: Kluwer), 193-226

Shu, F. H., Najita, J., Shang, H. & Li, Z.-Y. 2000, in Planets and Protostars IV, eds. V. Mannings, A. Boss, & S. Russell (Arizona: Univ of Arizona Press), p789

Stone, J. M. & Norman, M. L. 1992, ApJS, 80, 753

Syer, D. & Tremaine, S. 1996, MNRAS, 281, 925

Tafalla, M., Mardones, D., Myers, P. C., Caselli, P., Bachiller, R. & Benson, P. J. 1998, ApJ, 504, 900

Tomisaka, K. 1998, ApJ, 502, L163

——, 2000, ApJ, 528, L41

——, 2002, ApJ, 575, 306

Toomre, A. 1964, ApJ, 139, 1217

Toomre, A. 1982, ApJ, 259, 535

Ward-Thompson, D., Kirk, J. M., Crutcher, R. M. et al. 2000, ApJ, 537, L135

Wootten, A., Mangum J. G., Wiseman, J., & Fuller, G. A. 2003, AAS Bulletin 20.07

Zweibel, E. G. & Brandenburg, A. 1997a, ApJ, 478, 563

Zweibel, E. G. & Brandenburg, A. 1997b, ApJ, 485, 920

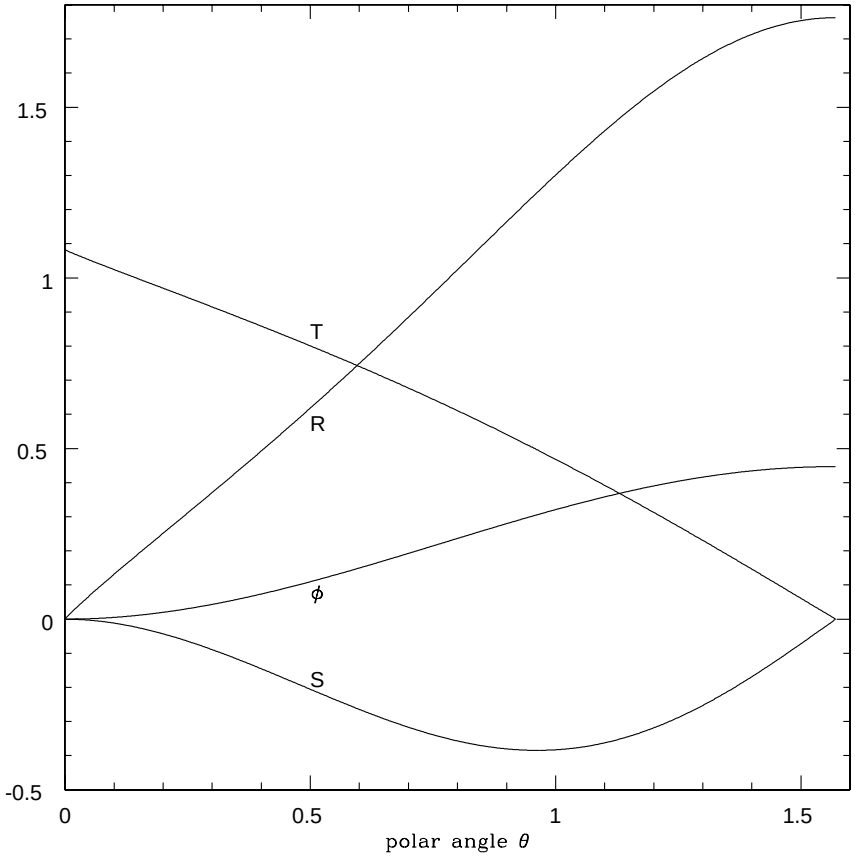

Fig. 1.— Plotted are the angular distribution functions for density R, magnetic flux ϕ, and two auxiliary functions S and T against the polar angle θ, for the combination of parameters $H_0 = 0.25$ and $v_0 = 0.25$. Note that both S and T go to zero at the equator $\theta = \pi/2$, which are the boundary conditions that fix the free parameters a_0 and b_0 in the expansions near the polar axis.

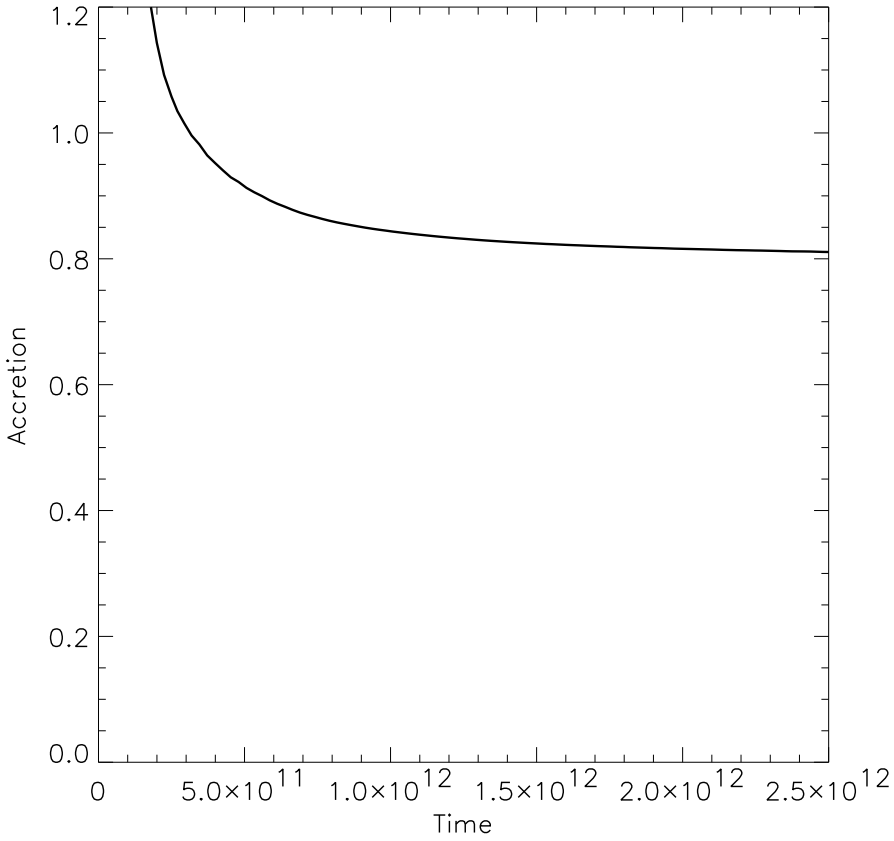

Fig. 2.— Central accretion rate constant $m_0 = G\dot{M}/(1 + H_0)a^3$ for the fiducial toroid of $H_0 = 0.25$ and $v_0 = 0.25$. Here we adopt a definition of $\dot{M}$ of the mass in the central cell divided by time (which differs from the instantaneous accretion rate shown in Fig. 3d of Paper I) to make the curve smooth. The initial peak is a numerical artifact from the way that the computation is started.

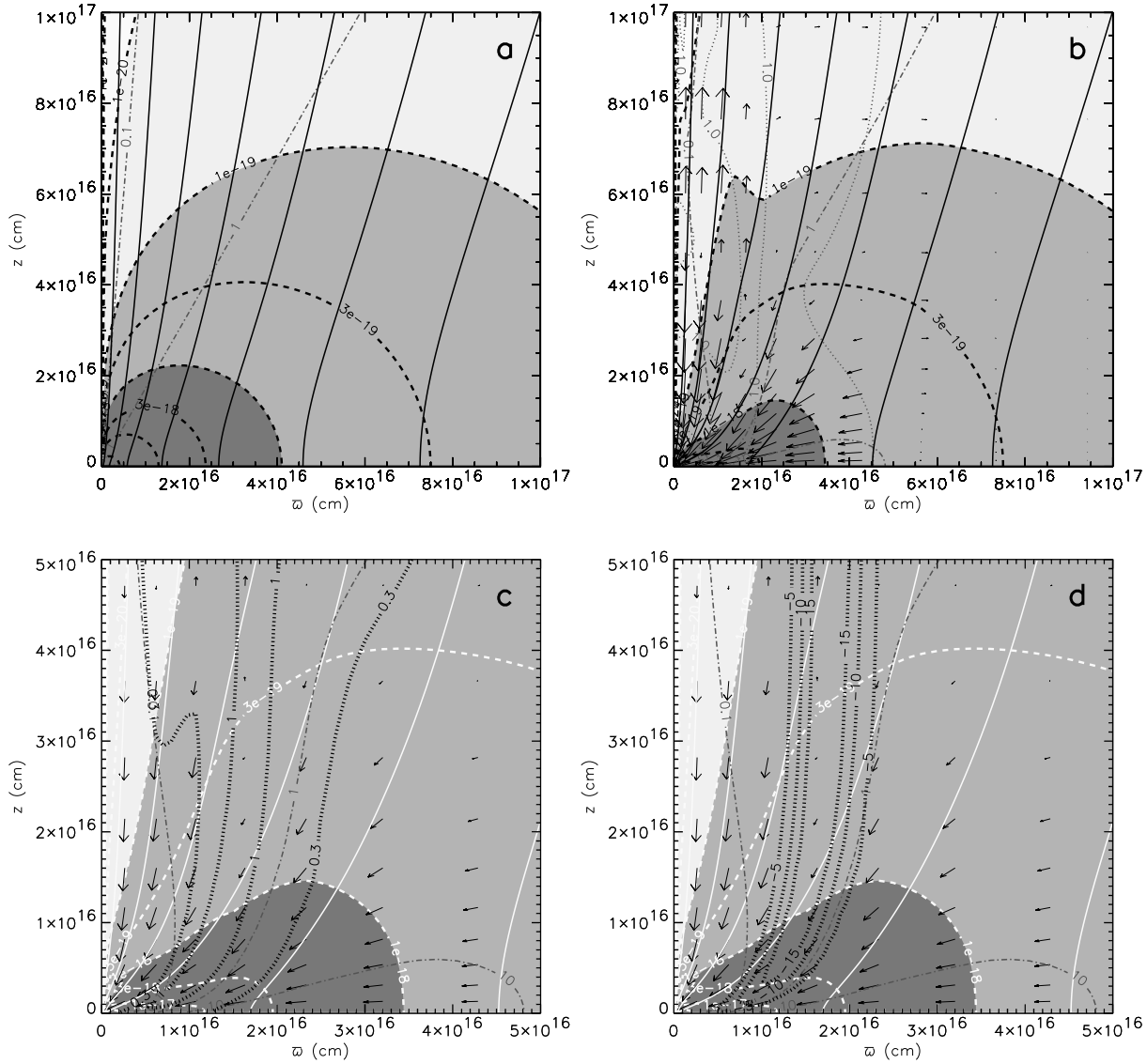

Fig. 3.— (a) The initial state of the fiducial $H_0 = 0.25$ and $v_0 = 0.25$ toroid at $t = 0$. (b) The collapse solution at time $t = 2.5 \times 10^{12}$ s. The contours of constant density (in units of g cm^{-3}) are plotted as dashed lines, with the shades highlighting the high density regions. The magnetic field lines are plotted as solid lines, with contours of constant β (dash-dotted) superposed. The velocity is shown by unit vectors, with its magnitude in units of the sound speed a given by the dotted lines. Panels (c) and (d) are closeup views of the inner region of panel (b), showing the contours of constant rotational speed and pitch angle of magnetic field, respectively, in heavy dotted lines.

Fig. 4.— Magnetic field lines for the fiducial case plotted at viewing angles of 60° and 0° (i.e., pole-on) inclination with respect to the magnetic pole. Innermost field lines shown in red, blue, and yellow are tied at the origin and pass through the pseudodisk as a split monopole configuration. Filed lines that thread through the midplane and have not yet been swept into the central mass point are shown in black.

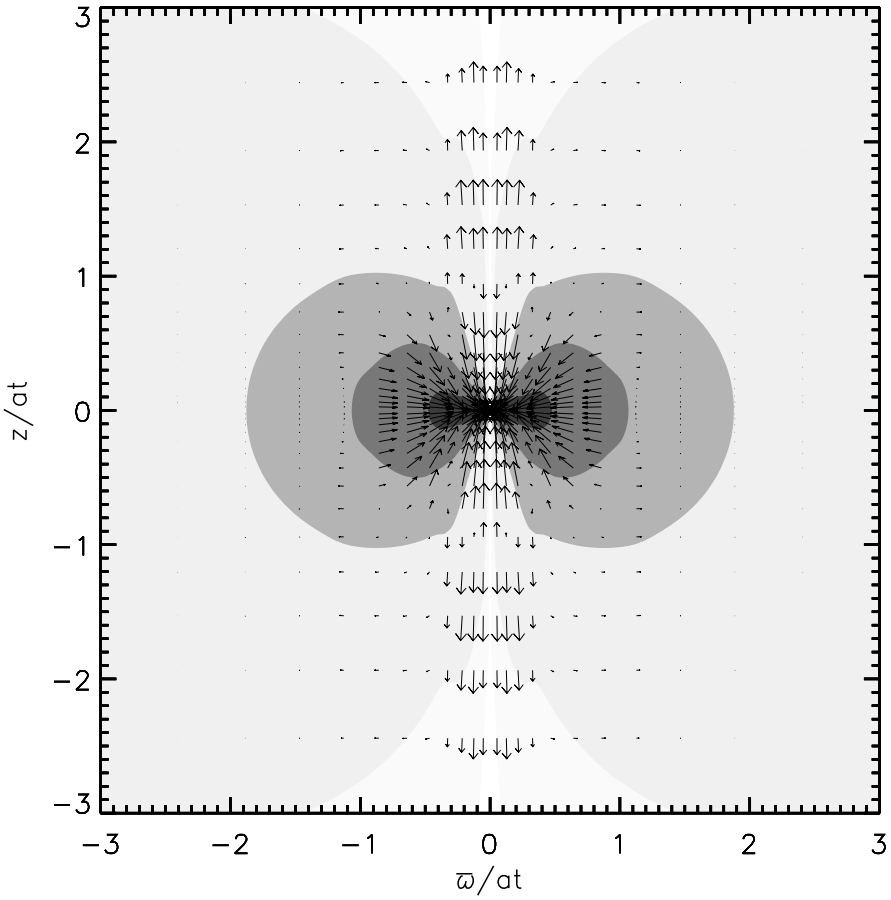

Fig. 5.— Velocity unit vectors (shown for every fifth cell) for the fiducial $H_0 = 0.25$, rotating toroid. Unit vectors are three dimensional; i.e., the rotational component pointing out of or into the plane of the page is not shown; thus, the displaced "unit vectors" have different lengths when they are projected into the meridional plane. The light, medium, and dark contours extending to approximately dimensionless cylindrical radius $\varpi \approx 0.5, 1$, and 2, respectively, correspond to reduced density $\alpha = 10, 1$, and 0.1, respectively.

Fig. 6.— Angular momentum redistribution due to magnetic braking. Plotted is the difference in angular momentum between the collapsed and initial configurations in similarity coordinates, $4\pi Gt\rho u_\varphi \varpi/a^2$, in the $\varpi/at - z/at$ plane, weighted by a factor of ϖ/at due to difference in ring volume at different radii. The quantities $4\pi Gt\rho u_\varphi \varpi/a^2$, ϖ/at, and z/at are shown on linear scales. The volume under the surface in a given region coordinate is proportional to the net change in angular momentum of that region from the initial pre-collapse state at $t = 0$.

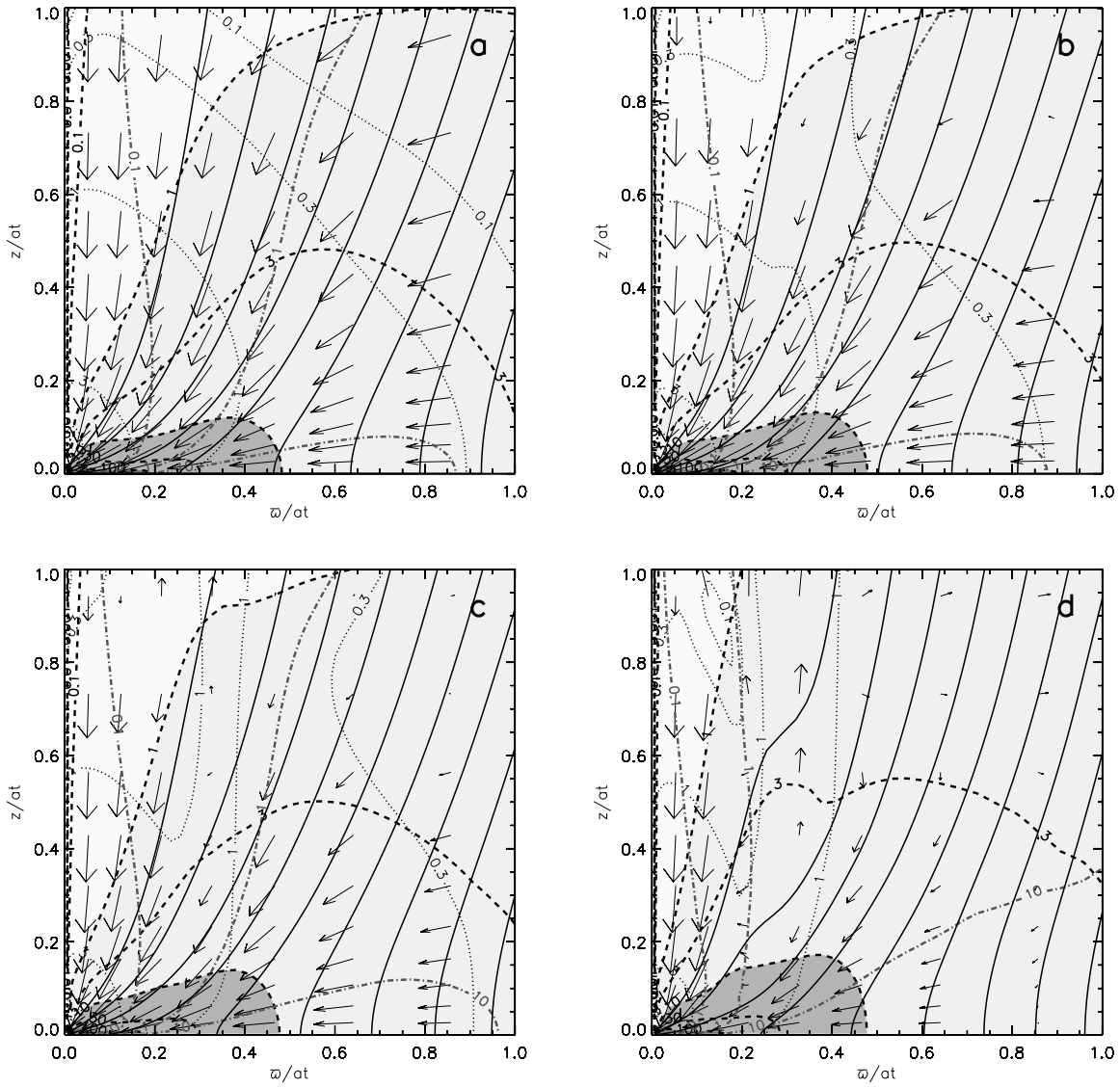

Fig. 7.— Plots of self-similar density, $4\pi G t^2 \rho$, velocity field, $\mathbf{u}/a$ and magnetic field, $\mathbf{B}G^{1/2}a/t$, lines for $H_0 = 0.25$ and $v_0 = 0, 0.125, 0.25$, and 0.5. The isodensity contours are plotted as dashed lines, with the shades highlighting the high density regions. The magnetic field lines are plotted as solid lines, with contours of constant β (dash-dotted) superposed. The velocity in every fifth cell is shown by unit vectors, with its magnitude given by the dotted contours. Field lines are not the same across all figures; examine the β contours for field strength. Notice that a centrifugally supported disk of dimensionless size $x_d \approx 0.25 v_0^2 \approx 0.06$ when $v_0 = 0.5$ in a nonmagnetic calculation has not appeared in the magnetized calculation of panel d.

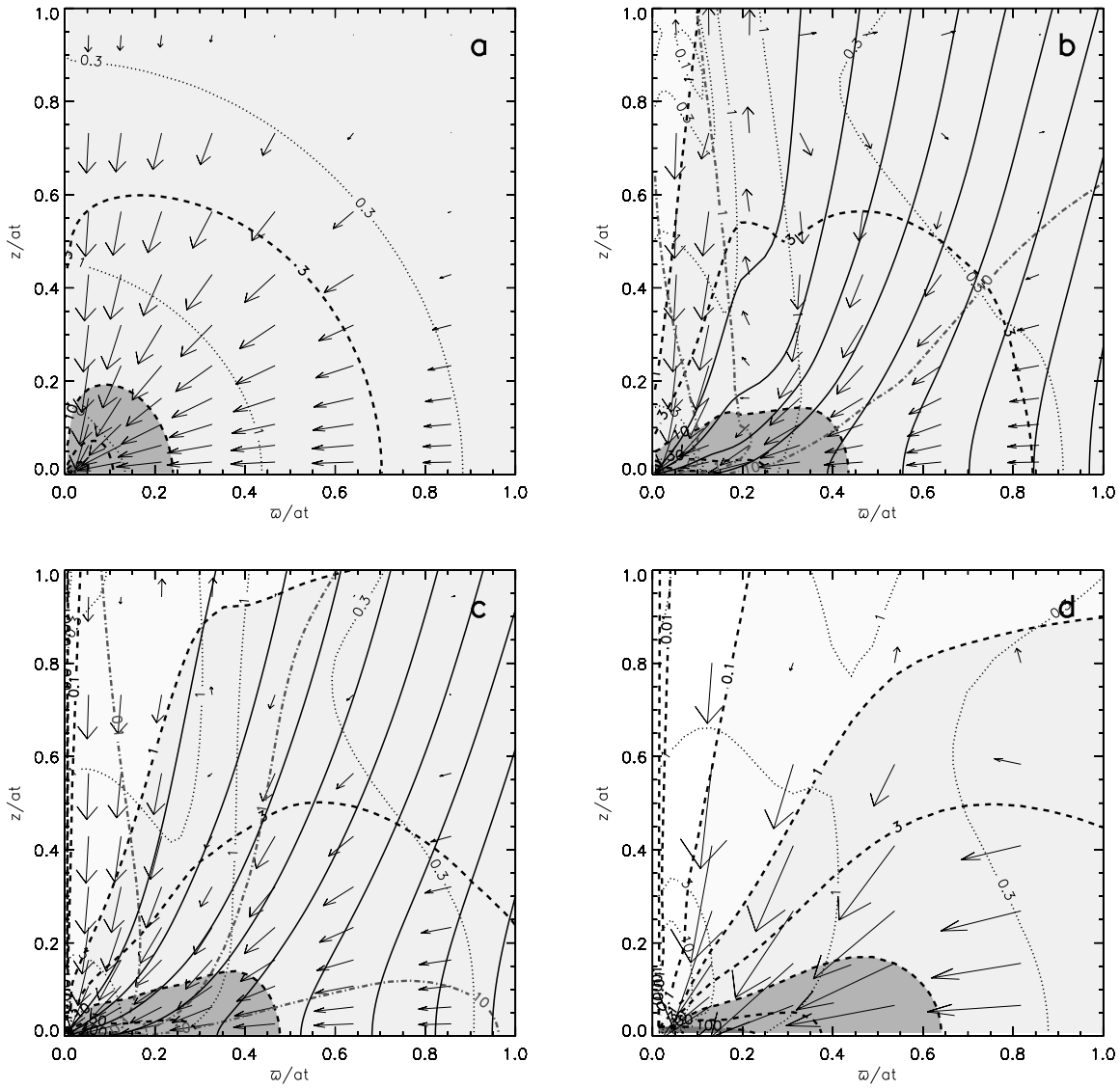

Fig. 8.— Plots of self-similar density, $4\pi G t^2 \rho$, velocity field, $\mathbf{u}/a$ and magnetic field, $\mathbf{B}G^{1/2}a/t$, lines for $v_0 = 0.25$ and different values of $H_0 = 0.03125, 0.125, 0.25$ and 0.5. The isodensity contours are plotted as dashed lines, with the shades highlighting the high density regions. The magnetic field lines are plotted as solid lines, with contours of constant β (dash-dotted) superposed. The velocity in every fifth cell is shown by unit vectors, with its magnitude given by the dotted contours. Field lines are not the same across all panels; the relative strength of magnetic field is indicated by the value of the plasma β.

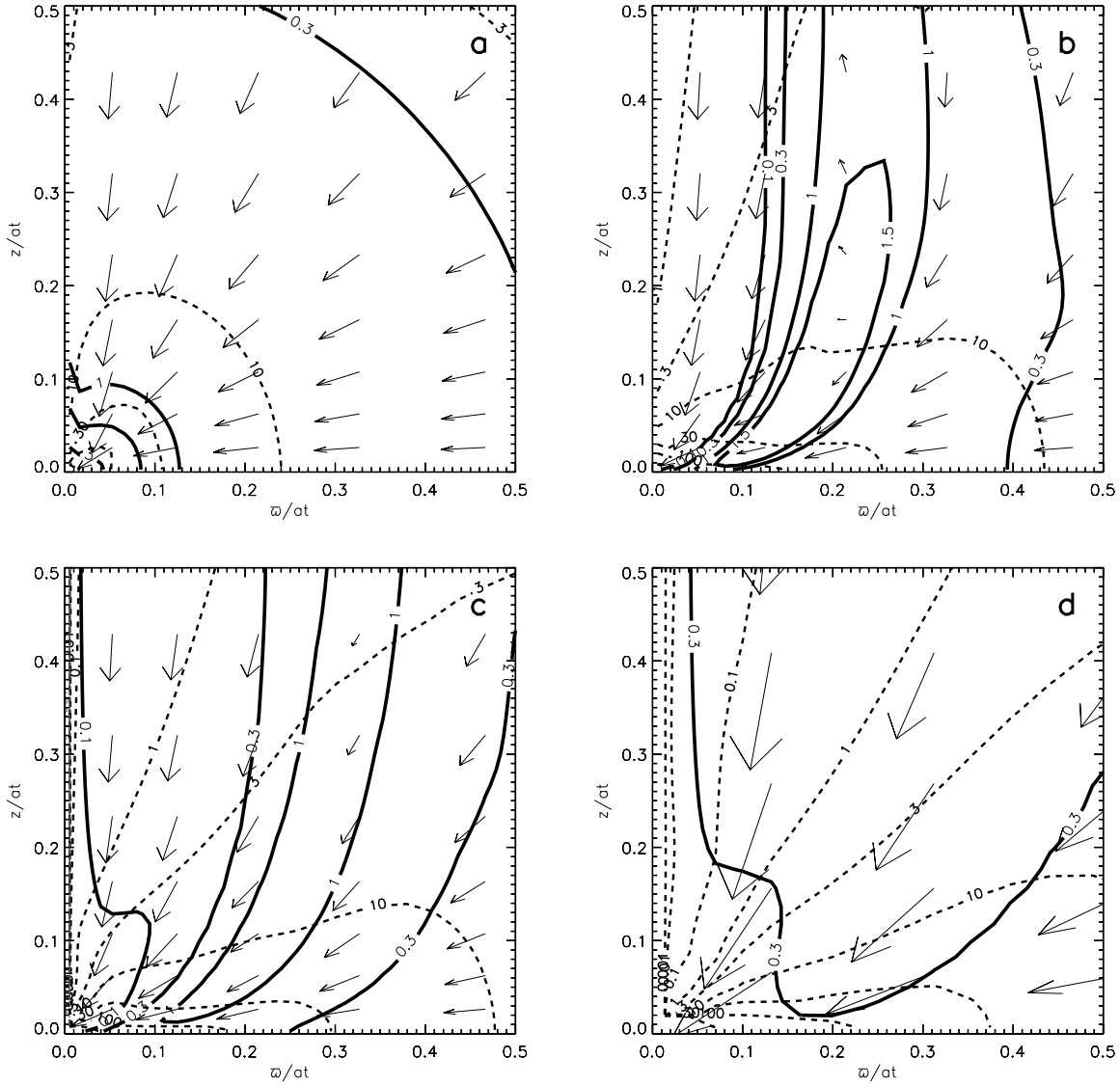

Fig. 9.— Plots of self-similar density (dashed contours) and rotational speed (solid contours) for $v_0 = 0.25$ and different values of $H_0 = 0.03125, 0.125, 0.25$ and 0.5. Comparing the rotational contours shows that the pseudodisk rotates more slowly in a more strongly magnetized case.

This figure "f4a.jpg" is available in "jpg" format from:

http://arXiv.org/ps/astro-ph/0311377v1

This figure "f4b.jpg" is available in "jpg" format from:

http://arXiv.org/ps/astro-ph/0311377v1

This figure "f6.jpg" is available in "jpg" format from:

http://arXiv.org/ps/astro-ph/0311377v1